IOCO 2026 Conference

The 1st International Online Conference on Optics

25–27 March 2026 | Online

MDPI

Laboratory Tests of a Low-Cost Multispectral Camera for Environmental Monitoring

Viktor Goryainov[1], Jacques Bernice Ngoua Ndong Avele[2]

[1] Department of Photonics, St. Petersburg Electrotechnical University "LETI"

[2] Department of Radiotechnical Systems, St. Petersburg Electrotechnical University "LETI"

INTRODUCTION & AIM

Multispectral and hyperspectral imaging is among the most valuable techniques for environmental monitoring. Affordable CMOS image sensors have served a wider adoption of multispectral cameras, including in educational and DIY projects. In this study, we present the laboratory tests of a low-cost multispectral camera designed for monitoring of vegetation.

The aim of the study was to evaluate the parameters that affect the performance of the multispectral camera: 1. field of view angular size; 2. depth of field and hyperfocal distance distributions; 3. spectral homogeneity of the field of view.

METHOD

The camera uses a set of interference filters for spectral separation, installed in two parallel wheels. The optical system creates a parallel beam of light before the filter, then forms the image on the surface of the OV5647 sensor [1].

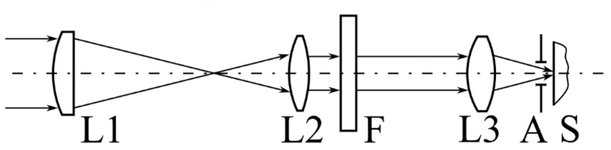

Fig. 1. The optical design of the camera: L1, L2, L3 – concave lenses; F – interference filter; A – aperture diaphragm; S – CMOS sensor.

1. The resulting field of view size and focal length of the camera were obtained by taking an image of an object of known size set at a predefined distance from the camera, then using the following expressions:

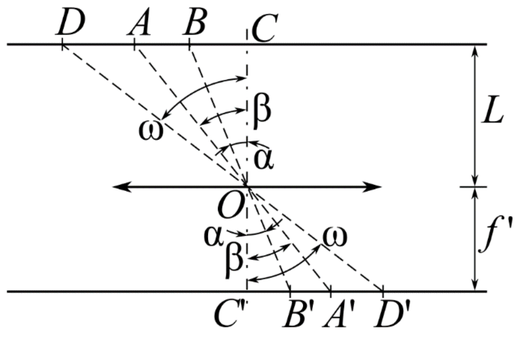

Fig. 2. Geometrical interrelations for the calculation of the field of view size and the focal length.

$$f' = L\frac{A'B'}{AB}; 2\omega = 2\,\mathrm{atan}\left(\frac{A'B'}{2f'}\right), \quad (1)$$

where L is the distance from the camera to the object; AB and $A'B'$ is the size of the object and of its image correspondingly; f' is the rear focal length of the camera; ω is half the angular size of the field of view.

2. The depth of field D was calculated for a given focus distance R and aperture K, as a difference between the least distance R_1 and the greatest distance R_2 at which an object would be pictured clearly:

$$D = R_2 - R_1;\ R_{1,2} = \frac{Rf'^2}{f'^2 \mp Kf'z \pm KRz}; K = \frac{f'}{Md_a}, \quad (2)$$

where z = 3 μm is the acceptable circle of confusion size (depends on the pixel size of the sensor); M is the transverse magnification of the optical system; d_a is the physical diameter of the aperture diaphragm [2]. The latter could be changed between 0.8 and 13.5 mm.

From the same considerations, the hyperfocal distance was calculated (the value of R that leads to $R_2 = \infty$):

$$H = \frac{f'^2}{Kz} + f'. \quad (3)$$

3. For the spectral homogeneity test, the camera was directed towards the overcast sky, and an image was obtained using the 580 nm interference filter. Since at this wavelength both the green and the red channel of the sensor are sensitive, then the ratio of the green and the red value was calculated for each pixel in the image:

$$RG(x,y) = \frac{Red(x,y)}{Green(x,y)}. \quad (4)$$

RESULTS & DISCUSSION

1. Using (1), the focal length of the camera f' was calculated to be equal to 58 mm, and its field of view angular size 2ω was equal to 3.6°. A narrow field of view makes our optical design similar to a telephoto lens, although the focal length is considerably shorter.

2. Considering the full-stop scale, the f-numbers from 1.4 (fully open diaphragm) to 22.0 (fully closed diaphragm) were available.

In Fig. 3, *a*, a distribution of the depth of field is shown in logarithmic scale ($\log_{10} D$) as a function of aperture value K and focus distance R, which was calculated using (2). The smallest value in the distribution was about 2 mm, measured from the sensor's surface. The white region in the upper right angle corresponds to hyperfocal distances, at which D becomes infinite.

Fig. 3, *b* shows the hyperfocal distance value H for each of the available f-numbers, ranging from 52.5 to 885.6 m for the smallest and the greatest aperture correspondingly.

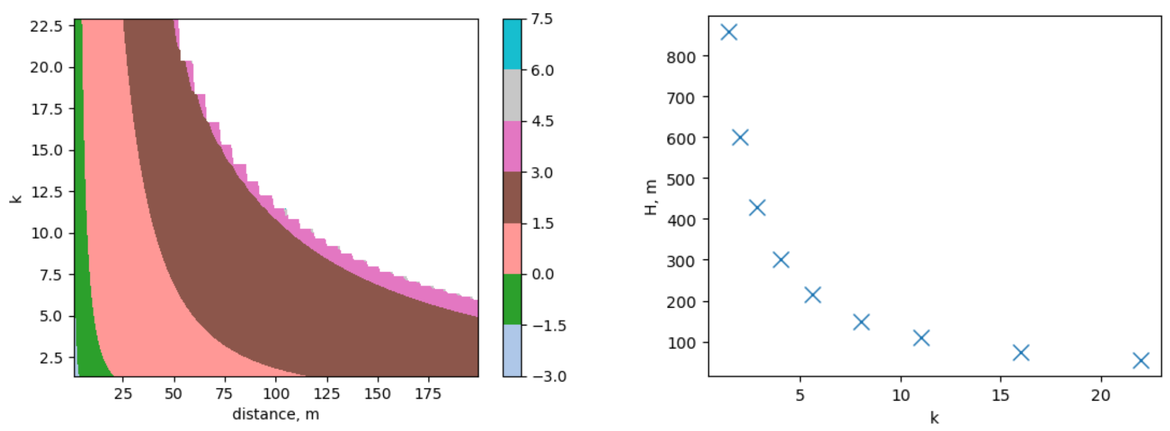

a *b*

Fig. 3. The resulting distributions of depth of field: *a* – the decimal logarithm of the depth of field $\log_{10} D$ as a function of aperture K and focus distance R; *b* – hyperfocal distance value H for the f-numbers available.

3. In Fig. 4, two examples of red-green ratio RG distribution are given. The distribution *a* was obtained during the adjustments and shows signs of vignetting (the left part of the image was darker in both the green and the red channel). The standard deviation σ_{RG} over the image was as high as 0.18. The distribution b is the result of the adjustments, and the standard deviation is as low as 0.03 in this case, which shows an acceptably small level of spectral inhomogeneity.

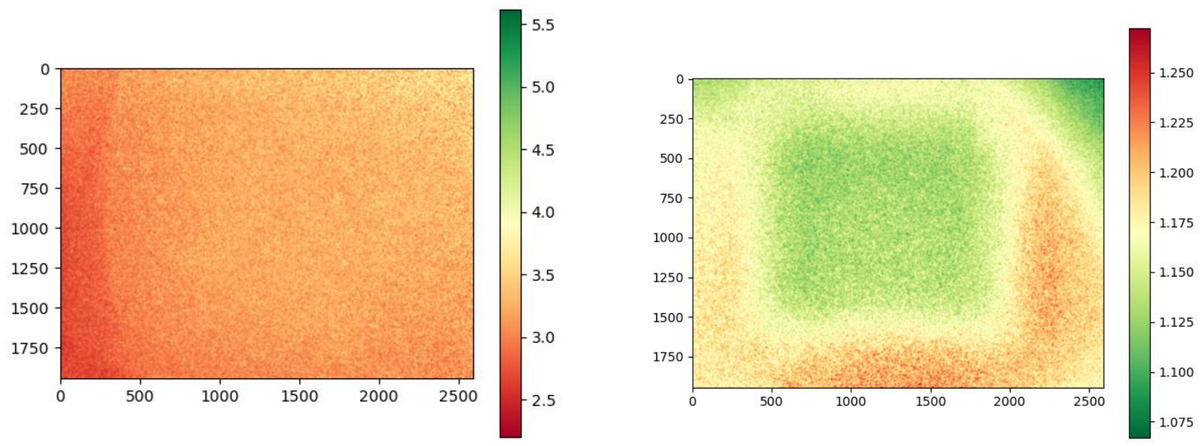

a *b*

Fig. 4. Red-green ratio distributions: *a* – in the process of adjustments, $\sigma_{RG} = 0.18$; *b* – after the adjustments, $\sigma_{RG} = 0.03$.

CONCLUSION

The laboratory tests have shown the suitability of the optical design selected for the multispectral camera. The camera's field of view size, depth of field values and the spectral homogeneity of the image are suitable for ecological monitoring of vegetation through the use of vegetation indices.

FUTURE WORK / REFERENCES

The future work will be concentrated on further refining the optical design of the camera, both through numerical modeling and laboratory experiments. Experimenting with other sensor models will allow to compare their performance and select the best option available.

[1] Goryainov, V.S.; Ngoua Ndong Avele, J.B.; Mazoya, A.B.; Tarasov, S.A. Portable multispectral camera for environmental monitoring. *J. Russ. Universities. Radioelectronics* **2025,** *28*, pp. 66–82. DOI: 10.32603/1993-8985-2025-28-5-66-82

[2] Allen, E.; Triantaphilidou, S. *The manual of photography*, 10th ed.; Focal Press: Burlington, USA, 2011; pp. 111–112.